Synsint Research Group

Available online at www.synsint.com

Synthesis and Sintering

ISSN 2564-0186 (Print), **ISSN** 2564-0194 (Online)

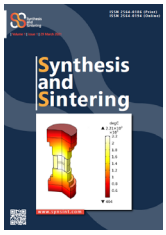

Research article

Influence of molybdenum content on the microstructure of spark plasma sintered titanium alloys

M. Saravana Kumar [a], **S. Rashia Begum** [b], **M. Vasumathi** [b], **Chinh Chien Nguyen** [c,d], **Quyet Van Le** [c,d,*]

[a] *Department of Mechanical Engineering, Mount Zion College of Engineering and Technology, Pudukkottai, Tamil Nadu, India*
[b] *Department of Mechanical Engineering, College of Engineering, Anna University, Chennai, Tamil Nadu, India*
[c] *Laboratory of Energy and Environmental Science, Institute of Research and Development, Duy Tan University, Da Nang 550000, Vietnam*
[d] *Faculty of Environmental and Chemical Engineering, Duy Tan University, Da Nang 550000, Vietnam*

ABSTRACT

Five titanium-based alloys containing 4, 8, 12, 16, and 20 wt% molybdenum additive were fabricated by spark plasma sintering process at 1200 °C. The samples were scrutinized in terms of relative density, phase evolution, and microstructural development. The relative density reached 99.9% with the molybdenum addition up to 16 wt% but slightly dropped in the sample with 20 wt% additive. In the specimens with 4 wt% Mo, molybdenum solved completely in the matrix and three different phase morphologies were observed, namely continuous α-Ti, laminar α-Ti, and very thin laminar β-Ti. With increasing Mo content to 20 wt%, widespread single β-Ti appeared alongside remained Mo and α-Ti. Ductile fracture mode was dominant in the samples with low Mo contents whilst it changed to brittle in the specimens with higher content of molybdenum.

KEYWORDS

Titanium
Molybdenum
Spark plasma sintering
Microstructure
Densification

OPEN ACCESS

1. Introduction

Titanium and Ti-based alloys have been recently considered as promising engineering materials, due to their excellent combination of properties. High specific strength, low density, excellent biocompatibility, and corrosion resistance, along with relatively low cost, make titanium and Ti-based alloys appropriate candidates for several applications including aerospace and chemical industries and, particularly, biomedical engineering [1–4]. In the latter case, although titanium and Ti-based alloys are currently used in both dental and bone implants, there are still several challenges to provide better biocompatibility and favorable long-term outcomes. The superiority of Ti-based bio-implants is derived from several factors. First of all, protective titanium dioxide film, which is instinctively formed on the titanium surface due to the high affinity of Ti to oxygen, and results in excellent corrosion resistance in biosystems. The electrochemical and physicochemical characteristics of the oxide film and its permanence in biological environments have a key role in the biocompatibility of titanium implants. Moreover, the osseointegration process enhances the presence of the oxide film [5], which means direct contact between the implant and viable bone with no soft-tissue layer [6]. It is also proven that Ti ions have minimum effects on the body metabolism and poisoning [7]. Therefore, most titanium-based implants can be used without any surface coatings, which decreases manufacturing costs [7]. Although there are some reports on applying commercially pure titanium (CP-Ti) in dentistry [8], shortcomings such as low wear resistance and machinability as well as process challenges in casting and welding of the material due to the high melting point of CP-Ti [9] promote the research works on design, modification, and processing of Ti-based alloys for biomedical applications [10–13]. Currently, TiNi

* Corresponding author. *E-mail address:* levanquyet@dtu.edu.vn (Q.V. Le)
Received 15 March 2021; Received in revised form 7 April 2021; Accepted 10 April 2021.

https://doi.org/10.53063/synsint.2021.1114

(Nitinol) and Ti-6Al-4V alloys are the most extensively used materials in biological applications [3, 4, 9, 14].

Nevertheless, there are many witness accounts against the benefits of some alloying elements, mainly due to unfavorable long-term effects caused by releasing the metal ions. For example, vanadium ions may cause cytotoxic effects and adverse reactions in some tissues, while aluminum ions can trigger neurological disorders, and nickel, which is occasionally considered allergenic [3, 7, 14–16]. In addition to toxicity, Ti-based implants may possibly lead to the resorption of neighboring bone tissues and the early collapse of the prosthetic devices because of a considerable mismatch between the elastic moduli of the host bone and that of the implants [2, 16]. Such a phenomenon, known as the stress shielding effect, leads to a heterogeneous distribution of load on the bone tissue and implant. In other words, it may lead to the health problems such as pain osteoporosis, bone mass loss, and even bone fractures [17]. The unconformity between Young's moduli of some Ti-based biomaterials (CP-Ti: 105 GPa and Ti-6Al-4V: 110 GPa) and those of human bones (10–30 GPa) was comparatively investigated by Zhao et al. [15]. Although several alloying elements do not cause any allotropic transformation in Ti-based alloys (α-stabilized alloys, hcp) and lead to higher strength and elastic modulus, some research studies have indicated that β-stabilized Ti-based alloys (bcc crystalline structure) show better formability [8] and lower Young's moduli [18].

Recently, β-stabilizer elements such as Sn, Mo, Hf, Zr, Ta, and Nb, which seem to be non-allergic and non-toxic, have been widely used to develop high strength and low elastic modulus Ti-based alloys for bone implant applications [19–21]. Among the mentioned alloying elements, molybdenum, niobium, and tantalum present the best combination of properties, including relatively high melting point, high strength, and low elastic modulus [2, 19–22]. Nevertheless, as the mentioned elements have relatively high densities, their binary alloys with Ti would be potentially heavy, which negatively affects their application in biomedical and orthopedic implants. Previous researches indicated that adequate contents of Mo, Nb, and Ta would be 8, 22, and 52 wt%, respectively, to achieve microstructures containing stabilized β-phase (after quenching) in Ti-Mo, Ti-Nb, and Ti-Ta binary alloys [2, 17]. Therefore, Mo seems to be the most effective β stabilizer, as a small amount of molybdenum (8 wt%) would have minimal effects on the overall density of the alloy [8].

Many research works were performed on the microstructure of Ti-Mo alloys and resulted in a clear understanding of the mechanism, steps, and transformation phenomena during the formation of β phase in such alloys [2, 3, 5, 8, 15, 16, 23–25]. Briefly, the microstructure of Ti-Mo alloys includes a combination of α, ά, ă, β+ω, ă+β+ω or β after quenching from β region, according to the Mo content [25]. Research indicates that a mixture of ă and β phases may result in a lower elastic modulus, whereas α increases the rigidity and ω promotes the brittleness of the alloy [2]. Since ά, ă, and ω phases mainly form during the equilibrium cooling of the β Ti-Mo alloys, the cooling process should be carried out as quenching. Nonetheless, remained transient phases are commonly found in the final microstructure of the alloy, based on the heat treatment, forming process, and especially the cooling rate of the final products. The presence of transient phases can result in lower mechanical properties and higher brittleness of the obtained components. Hence, many efforts, including modifications to manufacturing processes and finishing treatments, have been made to diminish the remained unfavorable phases [2, 16, 17,24–26]. Although most of the Ti-Mo implants are currently manufactured by casting method [2, 3, 8, 9, 16–18, 24] and inevitably require expensive finishing treatments, several attempts have recently focused on manufacturing methods based on Powder Metallurgy (PM) [27–29]. Besides disadvantages such as segregation and remained phases, the occurrence of casting defects is common in cast Ti-Mo alloys and can lead to an early failure of the components [30]. Particularly, bifilms as a result of entrapment phenomenon derived by turbulent flow during the casting process are known as one of the most destructive defects in oxidation-sensitive alloys, including Ti, Al, Mg, and Zn alloys [31–33]. Contrariwise, using powder metallurgy methods not only prevents the formation of bifilms and other casting defects, but also provides near-net shape components and eliminates the costly finishing treatments. However, common powder metallurgy methods (hot-pressing and pressureless sintering) have their own limitations, which mainly include excessive grain growth due to long-time heating (in order to obtain fully-dense material) and relatively expensive equipment.

In this paper, spark plasma sintering (SPS) method, as a recently developed PM technique, was used to produce Ti-Mo alloys from precisely combined powder mixtures. The method has many advantages, including very short dwelling time and homogenized heat and pressure distribution in the components, in comparison with common sintering techniques [34, 35]. The obtained results were then analyzed to indicate the influences of Mo content on the relative density, phase evolution, and microstructural characteristics of SPSed Ti-Mo alloys.

2. Experimental

2.1. Materials and process

Commercially pure titanium (purity > 98%; particle size < 60 μm) and molybdenum (purity > 99%; particle size < 20 μm) powders were used as raw materials. The chemical compositions of these powders are presented in Table 1, indicating that starting materials were highly pure. These powders were precisely weighed and mixed in a tubular mixer (4 hours, 60 rpm) to achieve Ti-Mo green mixtures. The green powder mixtures were then poured into cylindrical graphite die (diameter: 50 mm and thickness: 8 mm) lined with a flexible graphite foil. The specimens were finally sparked plasma sintered with a current on-off ratio of 12:2 and a pulse duration of 3.3 ms at 1200 °C for 5 min. The heating rate was 50 °C/min and the SPS process included a 50 MPa applied pressure and a vacuum < 1 Pa. Five samples were prepared and coded regarding the coding system presented in Table 2.

2.2. Characterization

To eliminate any contamination from the die, a 500 μm thick surface layer was removed from the samples. The bulk densities of the samples were measured with distilled water as the immersion medium based on the Archimedes method. Theoretical density was calculated based on the rule of mixtures and consequently applied in relative density (RD) calculations (Fig. 1). A routine grinding, polishing, and etching procedure were employed for surface preparation using Kroll's reagent (10 ml of HNO_3, 5 ml of HF, and 85 ml of H_2O). The microstructural study was carried out by an optical microscope (Olympus PMG3, Japan) and a field emission scanning electron microscope (Tescan Mira-3, Czech Republic) supplied with an energy-dispersive X-ray spectroscope (EDS) detector. X-ray diffractometry (XRD, Siemens D5000, Cu lamp, k = 1.54 Å, 30 mA, 40 kV) was employed for phase

Table 1. The compositions of starting powders.

Elements (wt%)	Ti	Mo	Fe	Al	V	O	H	N	Other
Ti powder	98.2	-	0.42	0.23	0.18	0.57	0.31	0.09	-
Mo powder	-	99.8	0.07	-	-	0.07	-	-	0.06

analysis. Differential scanning calorimetry (DSC) was carried out using a DSC (NETZSCH 404, Selb, Germany) device to study possible chemical reactions and phase transformations in the investigated material.

3. Results and discussion

Fig. 1 shows the relative density of the SPSed samples. Clearly, the relative density of the samples enhanced with the Mo content up to 16 wt% and then experienced a slight drop in 20 wt%. Although the chemical potential of diffusion increases at higher Mo contents, which leads to a better densification behavior of the alloys, Mo contents about 20 wt% (33 at%) and perhaps higher may result in a change in the diffusion behavior. Besides the chemical factors, differences in particle sizes of Ti and Mo powders may be considered as physical factor affecting the densification behavior of the Ti-Mo alloys. Smaller Mo particles can fill the vacant area between Ti particles, which will provide closer contacts between the particles and finally results in a relatively higher relative density of the sintered material. However, the sintering process with higher amounts of Mo evokes higher sintering temperatures, as the melting point of molybdenum is considerably higher than Ti. In the TM20 sample, therefore, it is reasonable to achieve a lower RD than that of the TM16 sample at 1200 °C.

Fig. 2 illustrates the phases detected in the XRD patterns of the samples. As it is clear, only peaks related to Ti (α & β) and Mo are detectable, indicating no chemical interactions between starting materials. However, increasing the Mo content leads to higher amounts of β-Ti and remained Mo. It is also notable that the Mo content about 20 wt% results in the highest amount of β-Ti together with detectable amounts of remained Mo.

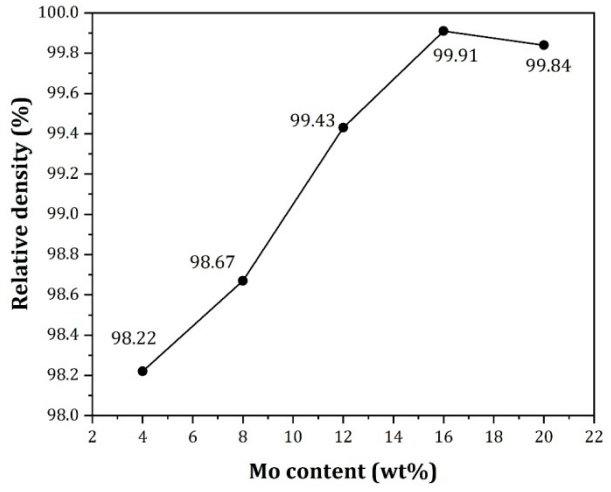

Fig. 1. The relative density of SPSed Ti-Mo samples vs. Mo content.

DSC analysis of TM20 powder sample is presented in Fig. 3, showing two peaks created owing to endothermic reactions. The first one, at 300-330 °C, was due to the evaporation of impurities in the initial Ti powder. The second one, which appeared close to 1000 °C, resulted from the transformation in the crystalline structure from α-Ti to β-Ti. However, as Mo is a β stabilizer, the second reaction could start at temperatures lower than the standard transformation temperature (around 500 °C) of α-Ti to β-Ti (882 °C).

The optical microscopy images of samples (Fig. 4) indicate that the availability of Mo element led to the stability of β-Ti at room temperature. Actually, this phase formed at a sintering temperature of 1200 °C, and needle-shaped α-phase (dark-colored) nucleated and precipitated into the β-phase (bright-colored). An increase in the concentration of Mo made it difficult for forming α phase, leading to β-phase coarsening. It is worthy to note that the presence of Mo, as a β stabilizer, decreases the martensite start temperature. Consequently, reaching a martensite microstructure will need a very fast quench speed to very low temperatures. Accordingly, as-sintered specimens in this research contained the equilibrium α + β phases with no martensite. Moreover, needle-shaped α-phases dispersed into β-grains can be observed in Fig. 4. Besides, the bright-colored area is also associated with Mo-rich phases. Actually, these Mo-rich zones formed around the agglomerated Mo powders, which were not able to dissolve completely into the matrix. It can be seen that the α-phase could not be formed in these areas. According to the Ti-Mo phase diagram [25], Mo as a β-isomorphous stabilizer can dissolve completely into titanium. Consequently, increasing the Mo content, namely dropping the phase transformation temperature, led to β stability at room temperature so that Mo-rich areas were 100% β-phase. A comparison of the optical micrographs of the samples reveals that the amounts of β and α + β were roughly the same in TM12, while β single-phase was predominant in TM16 and TM20 with increasing Mo concentration. Besides, dark dark-colored areas were containing compact α-phases into the β-zones in the specimens with high Mo content, including TM20. This phenomenon happened due to segregating Mo-poor areas after nucleating and growing β-grains.

Fig. 5 presents the SEM micrographs of the polished surfaces of the sintered specimens. The microstructure of the TM04 sample mainly includes α-Ti as the matrix (continuous phase) and small regions (marked area) containing a mixture of laminar β and α-Ti. Therefore, it seems that the diffusion of Mo atoms and the complete solution of molybdenum have resulted in the formation of a two-phase Ti-based alloy with three different phase morphologies, viz. continuous α-Ti,

Table 2. The coding system of the SPSed samples.

Code	TM04	TM08	TM12	TM16	TM20
Composition (wt% Mo)	4	8	12	16	20

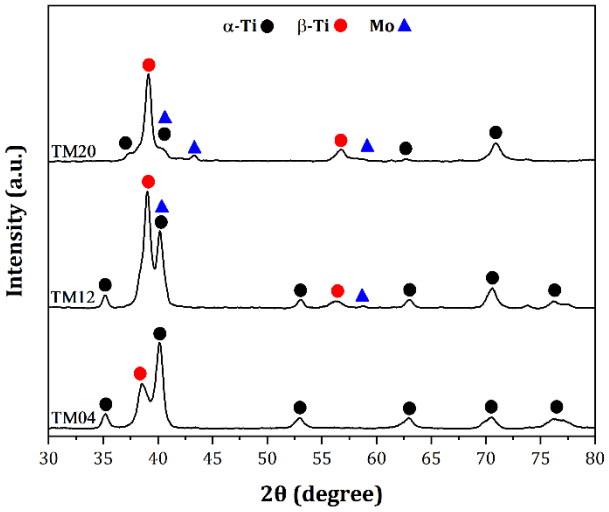

Fig. 2. XRD patterns of the SPSed samples.

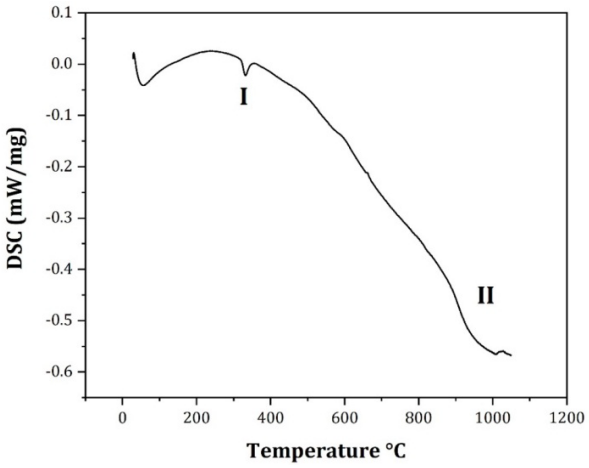

Fig. 3. DSC analysis of TM20 powder samples.

laminar α-Ti, and very thin laminar β-Ti. The latter formed as a consequence of insufficient Mo content, which had not completely stabilized the β-Ti.

As clearly seen in Fig. 5b, increasing the Mo content to 8 wt% not only caused a higher fraction of lamellar β-Ti (regions indicated by thin markers) but also developed the solid solution regions with a high concentration of Mo (indicated with thick markers). In addition, the concurrent formation of β-Ti layers, solid solution regions, and lower volume of porosity in the TM08 sample improved the relative density by around 0.5% compared with the TM04 specimen. The wide solid solution zones and lamellar α+β regions can be simply seen in the microstructure of the TM12 sample. Besides the mentioned phases, several remained Mo particles (indicated by black thick markers) are also visible, which are located inside the solid solution regions and match with the XRD pattern of the sample. The formation of higher amounts of β-Ti and also more solid solution regions are observable in the TM12 microscopic image. Although the formed interfaces between remained Mo particles and the matrix of the alloy should be investigated precisely (e.g. using TEM), it seems to have good compatibility with both Mo and matrix phases. Therefore, such remained Mo particles can promote strengthening via the pinning effect and increasing the mechanical properties due to decreasing the unfavorable grain growth. The EDS map analysis (Fig. 6) indicates the segregation of Mo in the Ti matrix. As it is evident, however, Mo dispersed uniformly all over the matrix, except in the zones containing

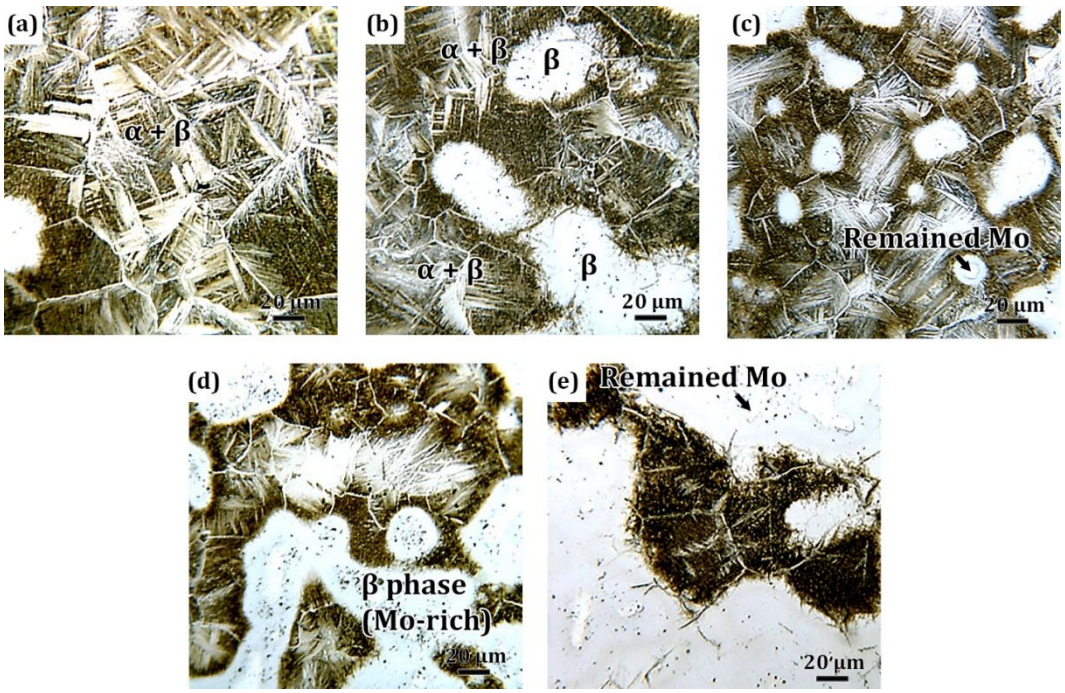

Fig. 4. Optical images of the polished surfaces of a) TM04, b) TM08, c) TM12, d) TM16, and e) TM20 samples.

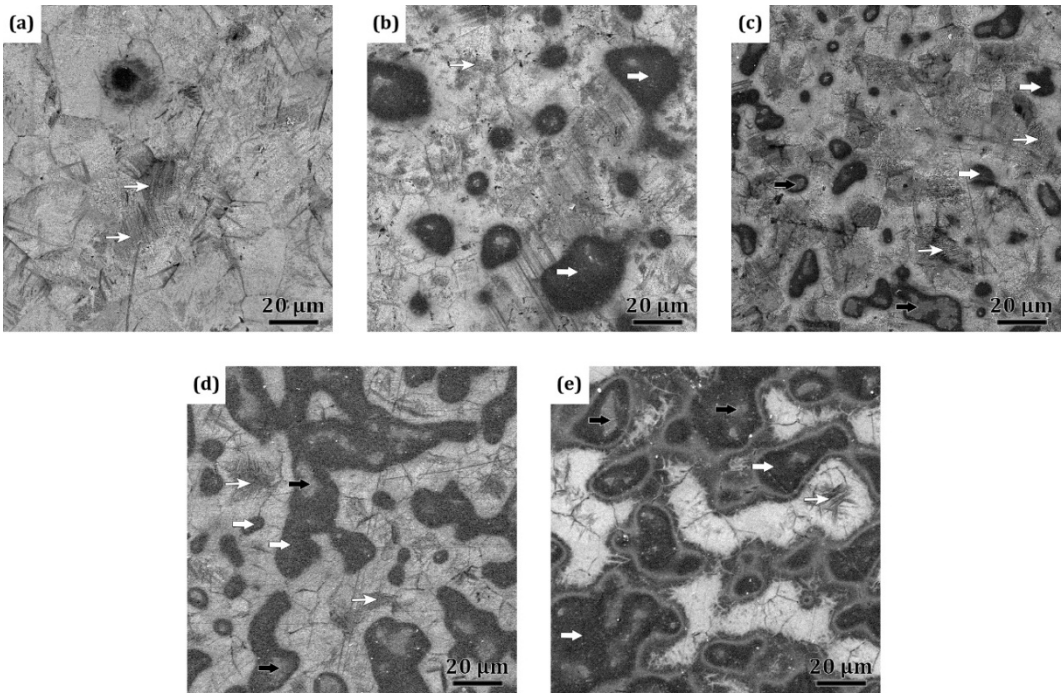

Fig. 5. SEM images of the polished surfaces of a) TM04, b) TM08, c) TM12, d) TM16, and e) TM20 samples.

agglomerated Mo particles due to the segregation. The microstructures of TM16 and TM20 samples (Figs. 5d and e) indicate higher fractions of remained Mo. Relatively thicker β-Ti layers have been formed in the TM16 sample (indicated by narrow white markers), but are not distributed homogeneously. The solid solution regions (indicated by thick white markers) are bigger and widely spread, and the amount of the hard remained Mo phase (indicated by black markers) is higher than those of TM08 and TM12 samples. The TM20 sample faced with insufficient diffusion of Mo atoms, which decreases the fraction of solid solution and β-Ti phases (indicated by white markers), as well as agglomerated Mo particles (indicated by black markers consisting of three distinct Mo particles). As it is utterly visible, such a mixed microstructure promotes higher porosity, which can lead to poor mechanical properties as the agglomerated Mo particles can act as potential cracks.

The fractographical approach can provide a clearer understanding of the microstructural evolution of Ti-Mo alloys during the SPS process. Therefore, SEM fractographs of TM04 to TM20 samples are presented in Fig. 7. As can be clearly seen in Fig. 7a, the fracture surface of the TM04 sample includes mixed inter/transgranular fractures. Hence, α-Ti is the dominant phase in this sample where the fracture surface mainly consists of fractured lamellas of α-Ti oriented in several directions. Such a morphology endorses the results of XRD patterns, as several relatively large α-Ti grains naturally promote a brittle fracture. Increasing the amount of Mo to 8 wt% apparently changes the fracture mode, as observed in the TM08 sample (Fig. 7b). The fracture surface includes ductile fractured grains with rough surfaces (white markers). The fracture mode in this specimen includes the brittle fracture of Mo-rich grains neutralized by a mixed fracture in lamellar α+β dual-phase regions. It appears that the

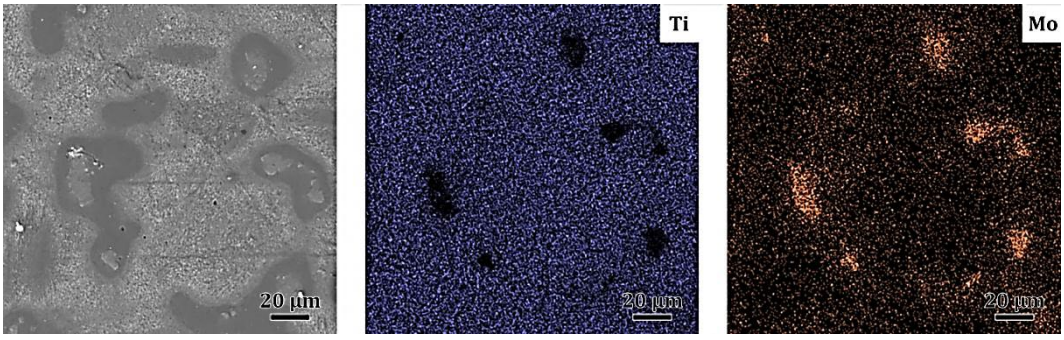

Fig. 6. SEM image of the polished surface of TM12 sample and corresponding EDS map results.

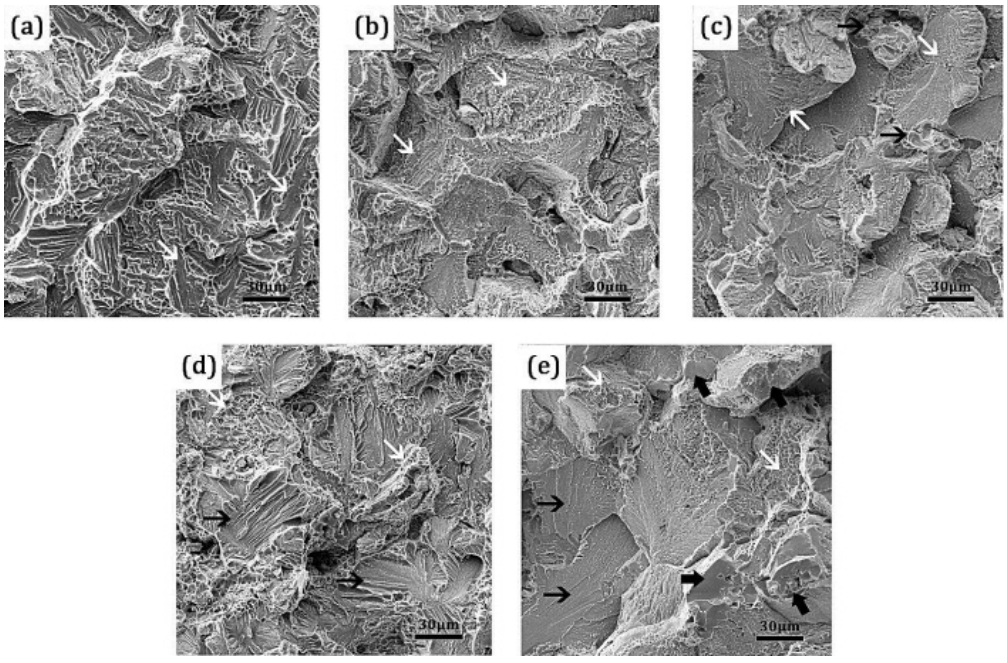

Fig. 7. SEM fractographs of a) TM04, b) TM08, c) TM12, d) TM16, and e) TM20 samples.

diffusion of Mo atoms led to the formation of high-strength equiaxed grains, which is accompanied by phase transformation from α-Ti to β-Ti, and resulted in mixed fracture mode in the TM08 sample. Although the further increase in the amount of Mo promotes higher amounts of β-Ti, it may cause remained Mo in the microstructure. Despite ductile fracture regions in Fig. 7c (indicated by white markers), there are some regions including brittle fracture (black markers). These regions mainly occurred due to the presence of remained Mo, which is not only naturally brittle but also remained un-sintered and can act as potential cracks. Since the remained Mo is small in size and well distributed, they usually cannot be considered as stress concentration sites but may act as grain boundary lockers (pinning effect) and avoid excessive grain growth.

As it can be clearly seen, the fracture surface of the TM16 sample (Fig. 7d) includes several brittle fracture sites (black markers), which are surrounded by ductile fracture regions (white markers). On the one hand, higher amounts of Mo than the TM12 sample causes higher remained Mo in the microstructure, and on the other hand, concentrated β-Ti phases (see Figs. 4d and 5d) results in compact colonies of α-Ti. While both α-Ti and remained Mo phases promote brittle fracture, un-sintered remained Mo phases can also act as potential cracks (although they decrease the grain growth). In the TM20 sample (Fig. 7e), the fracture surface indicates the intergranular fracture of remained Mo (thick black markers) caused by un-sintered and agglomerated Mo particles. Brittle fracture mode can also be seen in widespread regions (narrow black markers), whereas there are very small regions containing ductile fracture (white markers). Therefore, as it was mentioned before, higher fractions of Mo change the diffusion mode and lead to large β-Ti together with several remained unsolved Mo and α-Ti regions.

4. Conclusions

Titanium-based alloys, containing 4, 8, 12, 16, and 20 wt% molybdenum were manufactured by spark plasma sintering. The effects of alloying element (Mo) amounts were scrutinized on microstructural evolution and densification behavior of Ti-Mo alloys. The results showed that the Ti-16 wt% Mo alloy, spark plasma sintered at 1200 °C under 50 MPa for 5 min, had the highest relative density (99.91%). Complete dissolution of Mo took place at the lowest amount of Mo (4 wt%), yielding a two-phase Ti-based alloy with three various phase morphologies of continuous α-Ti, laminar α-Ti, and very thin laminar β-Ti. On the other hand, the highest amount of Mo (20 wt%) led to widespread single β-Ti formation together with continuous α-Ti and remained Mo (unsolved Mo).

CRediT authorship contribution statement

M. Saravana Kumar: Investigation, Writing – original draft.
S. Rashia Begum: Methodology, Project administration.
M. Vasumathi: Validation, Writing – review & editing.
Chinh Chien Nguyen: Supervision, Funding acquisition.
Quyet Van Le: Writing – review & editing.

Data availability

The data underlying this article will be shared on reasonable request to the corresponding author.

Declaration of competing interest

The authors declare no competing interests.

Funding and acknowledgment

The authors would like to thank the Indian and Vietnamese universities that were the foundation of this joint research collaboration.

References

[1] A. Sabahi Namini, M. Azadbeh, M. Shahedi Asl, Effect of TiB2 content on the characteristics of spark plasma sintered Ti–TiB w composites, Adv. Powder Technol. 28 (2017) 1564–1572. https://doi.org/10.1016/j.apt.2017.03.028.

[2] F.F. Cardoso, P.L. Ferrandini, E.S.N. Lopes, A. Cremasco, R. Caram, Ti–Mo alloys employed as biomaterials: Effects of composition and aging heat treatment on microstructure and mechanical behavior, J. Mech. Behav. Biomed. Mater. 32 (2014) 31–38. https://doi.org/10.1016/j.jmbbm.2013.11.021.

[3] Y. Chen, L. Xu, Z. Liu, F. Kong, Z. Chen, Microstructures and properties of titanium alloys Ti-Mo for dental use, Trans. Nonferrous Met. Soc. China. 16 (2006) s824–s828. https://doi.org/10.1016/S1003-6326(06)60308-7.

[4] C. Leyens, M. Peters, Titanium and Titanium Alloys: Fundamentals and Applications, John Wiley & Sons, Ltd. (2003). https://doi.org/10.1002/3527602119.

[5] N.T.C. Oliveira, G. Aleixo, R. Caram, A.C. Guastaldi, Development of Ti–Mo alloys for biomedical applications: Microstructure and electrochemical characterization, Mater. Sci. Eng. A. 452–453 (2007) 727–731. https://doi.org/10.1016/j.msea.2006.11.061.

[6] R. Adell, U. Lekholm, B. Rockler, P.-I. Brånemark, A 15-year study of osseointegrated implants in the treatment of the edentulous jaw, Int. J. Oral Surg. 10 (1981) 387–416. https://doi.org/10.1016/S0300-9785(81)80077-4.

[7] M. Abdel-Hady Gepreel, M. Niinomi, Biocompatibility of Ti-alloys for long-term implantation, J. Mech. Behav. Biomed. Mater. 20 (2013) 407–415. https://doi.org/10.1016/j.jmbbm.2012.11.014.

[8] W. Ho, C. Ju, J. Chern Lin, Structure and properties of cast binary Ti–Mo alloys, Biomaterials. 20 (1999) 2115–2122. https://doi.org/10.1016/S0142-9612(99)00114-3.

[9] E.-B. Lee, M.-K. Han, B.-J. Kim, H.-J. Song, Y.-J. Park, Effect of molybdenum on the microstructure, mechanical properties and corrosion behavior of Ti alloys, Int. J. Mater. Res. 105 (2014) 847–853. https://doi.org/10.3139/146.111092.

[10] Y. Li, C. Yang, H. Zhao, S. Qu, X. Li, Y. Li, New Developments of Ti-Based Alloys for Biomedical Applications, Materials (Basel). 7 (2014) 1709–1800. https://doi.org/10.3390/ma7031709.

[11] M. Niinomi, M. Nakai, Titanium-Based Biomaterials for Preventing Stress Shielding between Implant Devices and Bone, Int. J. Biomater. 2011 (2011) 1–10. https://doi.org/10.1155/2011/836587.

[12] P. Rocher, L. El Medawar, J.-C. Hornez, M. Traisnel, J. Breme, H. Hildebrand, Biocorrosion and cytocompatibility assessment of NiTi shape memory alloys, Scr. Mater. 50 (2004) 255–260. https://doi.org/10.1016/j.scriptamat.2003.09.028.

[13] E. Eisenbarth, D. Velten, M. Müller, R. Thull, J. Breme, Biocompatibility of β-stabilizing elements of titanium alloys, Biomaterials. 25 (2004) 5705–5713. https://doi.org/10.1016/j.biomaterials.2004.01.021.

[14] D.R.N. Correa, F.B. Vicente, R.O. Araújo, M.L. Lourenço, P.A.B. Kuroda, et al., Effect of the substitutional elements on the microstructure of the Ti-15Mo-Zr and Ti-15Zr-Mo systems alloys, J. Mater. Res. Technol. 4 (2015) 180–185. https://doi.org/10.1016/j.jmrt.2015.02.007.

[15] X. Zhao, M. Niinomi, M. Nakai, J. Hieda, Beta type Ti–Mo alloys with changeable Young's modulus for spinal fixation applications, Acta Biomater. 8 (2012) 1990–1997. https://doi.org/10.1016/j.actbio.2012.02.004.

[16] Y.-L. Zhou, D.-M. Luo, Microstructures and mechanical properties of Ti–Mo alloys cold-rolled and heat treated, Mater. Charact. 62 (2011) 931–937. https://doi.org/10.1016/j.matchar.2011.07.010.

[17] W. Zhang, Y. Liu, H. Wu, M. Song, T. Zhang, et al., Elastic modulus of phases in Ti–Mo alloys, Mater. Charact. 106 (2015) 302–307. https://doi.org/10.1016/j.matchar.2015.06.008.

[18] Y.L. Zhou, M. Niinomi, T. Akahori, Effects of Ta content on Young's modulus and tensile properties of binary Ti–Ta alloys for biomedical applications, Mater. Sci. Eng. A. 371 (2004) 283–290. https://doi.org/10.1016/j.msea.2003.12.011.

[19] M. Niinomi, Recent metallic materials for biomedical applications, Metall. Mater. Trans. A. 33 (2002) 477–486. https://doi.org/10.1007/s11661-002-0109-2.

[20] E. Delvat, D.M. Gordin, T. Gloriant, J.L. Duval, M.D. Nagel, Microstructure, mechanical properties and cytocompatibility of stable beta Ti–Mo–Ta sintered alloys, J. Mech. Behav. Biomed. Mater. 1 (2008) 345–351. https://doi.org/10.1016/j.jmbbm.2008.01.006.

[21] P.L. Ferrandini, F.F. Cardoso, S.A. Souza, C.R. Afonso, R. Caram, Aging response of the Ti–35Nb–7Zr–5Ta and Ti–35Nb–7Ta alloys, J. Alloys Compd. 433 (2007) 207–210. https://doi.org/10.1016/j.jallcom.2006.06.094.

[22] G. He, J. Eckert, Q.L. Dai, M.L. Sui, W. Löser, et al., Nanostructured Ti-based multi-component alloys with potential for biomedical applications, Biomaterials. 24 (2003) 5115–5120. https://doi.org/10.1016/S0142-9612(03)00440-X.

[23] Y. Takemoto, I. Shimizu, A. Sakakibara, M. Hida, Y. Mantani, Tensile Behavior and Cold Workability of Ti-Mo Alloys, Mater. Trans. 45 (2004) 1571–1576. https://doi.org/10.2320/matertrans.45.1571.

[24] M. Sabeena, S. Murugesan, R. Mythili, A.K. Sinha, M.N. Singh, et al., Studies on ω Phase Formation in Ti-Mo Alloys Using Synchrotron XRD, Trans. Indian Inst. Met. 68 (2015) 1–6. https://doi.org/10.1007/s12666-014-0426-3.

[25] J.L. Murray, The Mo−Ti (Molybdenum-Titanium) system, Bull. Alloy Phase Diagr. 2 (1981) 185–192. https://doi.org/10.1007/BF02881476.

[26] C.H. Wang, M. Liu, P.F. Hu, J.C. Peng, J.A. Wang, et al., The effects of α″ and ω phases on the superelasticity and shape memory effect of binary Ti-Mo alloys, J. Alloys Compd. 720 (2017) 488−496. https://doi.org/10.1016/j.jallcom.2017.05.299.

[27] G. Dercz, I. Matuła, M. Zubko, A. Liberska, Structure Characterization of Biomedical Ti-Mo-Sn Alloy Prepared by Mechanical Alloying Method, Acta Phys. Pol. A. 130 (2016) 1029–1032. https://doi.org/10.12693/APhysPolA.130.1029.

[28] Z. Gao, H. Luo, Q. Li, Y. Wan, Preparation and Characterization of Ti-10Mo Alloy by Mechanical Alloying, Metallogr. Microstruct. Anal. 1 (2012) 282–289. https://doi.org/10.1007/s13632-012-0045-5.

[29] H. Hosokawa, K. Kato, K. Shimojima, A. Matsumoto, Microstructural Evolution of Ti-Mo-Ni-C Powder by Mechanical Alloying, Mater. Trans. 50 (2009) 117–122. https://doi.org/10.2320/matertrans.MRA2008280.

[30] M.T. Jovanović, B. Dimčić, I. Bobić, S. Zec, V. Maksimović, Microstructure and mechanical properties of precision cast TiAl turbocharger wheel, J. Mater. Process. Technol. 167 (2005) 14–21. https://doi.org/10.1016/j.jmatprotec.2005.03.019.

[31] Y. Liu, W. Wei, K. Zhou, L. Chen, H. Tang, Microstructures and mechanical behavior of PM Ti-Mo alloy, J. Cent. South Univ. Technol. 10 (2003) 81–86. https://doi.org/10.1007/s11771-003-0043-5.

[32] J. Campbell, Entrainment defects, Mater. Sci. Technol. 22 (2006) 127–145. https://doi.org/10.1179/174328406X74248.

[33] B. Nayebi, A. Bahmani, M. Shahedi Asl, A. Rasooli, M. Ghasemi Kakroudi, M. Shokouhimehr, Characteristics of dynamically formed oxide films in aluminum–calcium foamable alloys, J. Alloys Compd. 655 (2016) 433–441. https://doi.org/10.1016/j.jallcom.2015.09.200.

[34] A. Sabahi Namini, M. Shahedi Asl, S.A. Delbari, Influence of Sintering Temperature on Microstructure and Mechanical Properties of Ti–Mo–B4C Composites, Met. Mater. Int. 27 (2019) 1092–1102. https://doi.org/10.1007/s12540-019-00469-y.

[35] S.A. Delbari, A. Sabahi Namini, M. Shahedi Asl, Hybrid Ti matrix composites with TiB2 and TiC compounds, Mater. Today Commun. 20 (2019) 100576. https://doi.org/10.1016/j.mtcomm.2019.100576.